

# **ADVANCED COMPOSITES III: Expanding the Technology**

*Proceedings of the Third Annual Conference on  
Advanced Composites  
15-17 September 1987  
Detroit, Michigan*

*Sponsors:*



ASM INTERNATIONAL



Engineering Society of Detroit

*Endorsing Sponsor:*



Society of Plastics Engineers

Published by



# MATERIAL DESIGN PARAMETERS AFFECTING THE COMPRESSIVE AND BENDING LOAD CAPACITY OF DELAMINATED ANGLE-PLY COMPOSITES

D.W. Schmueser, G.A. Kardomateas, G.T. Mase

General Motors Research Laboratories  
Warren, MI USA

## ABSTRACT

This study is directed at experimentally and analytically characterizing the effects which material type and angle-ply lay-up have on delamination failure mechanism of continuous fiber composites. Axial impact tests were performed on graphite/epoxy, Kevlar/epoxy, and glass/epoxy tubes to characterize failure modes and energy absorption levels. Experimental studies were also completed to study the bending performance of composite beams. The tests showed that delamination is the primary failure mechanism on the compressively-loaded beam face. In order to determine the manner in which angle-ply construction and material type affects delamination stability and growth on this compressive face, a one-dimensional beam-plate model of the delamination was formulated. Using this model, the phenomenological aspects of delamination failure were investigated over a broad range of values for angle-ply construction.

THE IMPORTANCE OF MATERIAL SELECTION to improve the impact performance of automotive and aerospace structures is evident through increased design requirements that govern crashworthiness behavior. With the recent increased emphasis on lightweight vehicle structures, the use of composite materials in automotive design has created the need to characterize and understand failure of composites subjected to compression and bending loads. This understanding should include the various material design parameters that govern composite behavior.

Delamination (separation of adjoining plies) is a stiffness and strength reduction mechanism encountered in laminated composites subjected to compressive loading. This mode of failure is of particular significance since it can control the ultimate load capacity and postbuckling behavior of laminates. Recent work that has dealt with the static crush of composite tubes has shown that delamination and interlaminar shear failure govern the energy absorption capacity of lami-

nated composites. Farley [1] conducted a study on the energy absorption characteristics of selected composite materials systems and aluminum. Static compression tests were conducted on tape and woven glass/epoxy (G<sub>2</sub>/Ep), Kevlar/Epoxy (K/Ep), and graphite/epoxy (Gr/Ep) tubes. The Gr/Ep and G<sub>2</sub>/Ep tubes failed in a brittle fracture mode, whereas the K/Ep tubes failed via delamination buckling. Specific energy absorption values for the G<sub>2</sub>/Ep and K/Ep materials were less than the Gr/Ep. Thornton [2] examined the energy absorption of statically compressed, small diameter G<sub>2</sub>/Ep, K/Ep and Gr/Ep tubes. Gr/Ep and G<sub>2</sub>/Ep tubes had brittle failure modes dominated by interlaminar shear failure and fiber fracture.

The present study focuses on the effects which material type and angle-ply lay-up have on the failure characteristics and energy absorption capacity of composite tubes subjected to axial impact loads and composite rectangular beams subjected to bending loads. A one-dimensional beam-plate model of the delamination failures predominant in these tests is applied to investigate the phenomenological aspects of delamination buckling and growth.

## AXIAL IMPACT CHARACTERIZATION TESTS

TUBE GEOMETRY AND MATERIALS - Laminated composite tubes with nominal diameter and length equal to 100 mm and 305 mm, respectively, were fabricated using T-300/5208, Kevlar 49/5208, and S-Glass/5208 unidirectional prepreg tape. Nominal cured ply thicknesses for these materials are listed in Table 1. Each of the drop specimens was fabricated using an 8-ply lamination sequence of  $(0_2/+ - a)_s$ , with  $a$  equal to 0, 30, 45, 60 and 90 degrees with respect to the cylinder axis. Only the lay-up angle,  $a$ , was varied for this study. The effect of changing the laminate stacking sequence was not considered. A summary of the laminate ply orientation and wall thicknesses is given in Table 2.

DROP TOWER TEST PROCEDURES - The GMR drop test facility is shown in Fig. 1 and consists of a 930 mm x 930 mm drop platform weighing 145 kg with an attached test specimen. The test speci-

men is secured with hot-melt adhesive into the machined grooves of a mounting plate which is bolted to the underside of the drop platform. The platform is guided during free-fall by four tension cables which are located at each platform corner.

For the present test program, the drop platform was raised to a predetermined height which gave an impact velocity of 5.5 m/sec. The platform was released with a grip latch pin mechanism that was extracted with two manually-activated electronic solenoids. The impact tests were filmed with a high-speed Redlake Hycam-2 movie camera at a filming rate of 8000 frames per second in full-frame operating mode.

After a series of drop tests are completed, digitized data representing the force-time and velocity-time histories of the impact events are numerically processed to determine the force-deflection response for each test. Signals from three load cells located beneath an impact plate (Fig. 1) are summed and amplified to give the force-time history. Velocity-time histories are obtained from square-wave pulses output from a magnetic pick-up device which follows a finely machined slotted strip as the drop tower falls. Discrete velocity points obtained from analyzing the square wave data are fitted with a least square spline curve. The spline curve is then numerically integrated to obtain the deflection-time history.

The resulting force-deflection response,  $F(\delta)$ , is used to compute specific energy absorption values for drop specimens. Representative force-deflection curves for composite and metallic tubes are illustrated in Fig. 2. Specific energy is defined by Eq. (1) as the ratio of the energy dissipated during impact to the crushed tube weight.

$$E_s^c = \frac{\int_0^{\delta_c} F(\delta) ds}{\delta_c \cdot A_s \cdot \rho} \quad (1)$$

In Eq. (1),  $\delta_c$  is the tube crush,  $A_s$  is the cross-sectional area, and  $\rho$  is the material density. Previous investigators have used the mean collapse,  $P_m$ , to approximate the specific energy absorption by the following equation.

$$E_s^c = \frac{P_m}{A_s \cdot \rho} \quad (2)$$

The present study uses numerical spline integration to more accurately compute the specific energy defined by Eq. (1).

**AXIAL IMPACT TEST RESULTS** - Fifty impact tests of composite tubes were completed. Each of the unidirectional tubes listed in Table 2 was tested once because of their relatively low energy absorption. Tests for the angle-ply G2/Ep and K/Ep tubes were each repeated four times, while tests for the angle-ply Gr/Ep tubes were each repeated three times. Impact data for two (0<sub>2</sub>/+ - 45)<sub>s</sub> G2/Ep tubes was disregarded because of instrumentation failure.

Specific energy results computed from the force-deflection curves of all the (0<sub>2</sub>/+ - a)<sub>s</sub> tubes are shown in Fig. 3. The results varied significantly as a function of material type and ply orientation. For each type of continuous fiber composite, a dramatic increase in specific energy absorption is achieved as the laminate ply orientation is varied from unidirectional to angle-ply. The Gr/Ep and K/Ep materials exhibited maximum specific energy absorption values for the (0<sub>2</sub>/+ - 60)<sub>s</sub> laminates, whereas the G2/Ep material had maximum energy absorption for the (0<sub>2</sub>/90<sub>2</sub>)<sub>s</sub> laminate. The angle-ply Gr/Ep tubes absorbed more energy than the K/Ep or G2/Ep tubes. This result is in agreement with the findings of Farley [1]. The present results show the K/Ep material to have significantly greater specific energy absorption than the G2/Ep material for a values of 30-60 degrees. Farley found the static energy absorption of the K/Ep and G2/Ep materials to be similar for all his ply orientations.

The specific energy absorption values were analyzed statically to determine the scatter for the experimental data. The confidence interval is defined by

$$C.I. = t_{\nu} \left[ \frac{(\text{Std. Dev})^2}{n} \right]^{1/2} \quad (3)$$

where  $t$  is the value of the students  $t$ -distribution for the number of degrees of freedom at a 95 percent confidence interval, and  $n$  is the number of test samples. A weighted least squares regression analysis [3] was completed to take into account the differences in sample size among the test groups. The results of the least square analysis, as summarized in Table 3, show that data scatter is minimum for the 45 degree tubes and maximum for the 90 degree tubes for each of the three types of composites.

Representative curves for impact force as a function of crush distance are illustrated in Fig. 2 for (0<sub>2</sub>/+ - 60)<sub>s</sub> composites, mild steel, and aluminum alloy. Figure 2 shows the post-peak force levels for Gr/Ep to be significantly greater than the G2/Ep and K/Ep materials. The post-peak force levels for the (0<sub>2</sub>/+ - 60)<sub>s</sub> Gr/Ep laminates are shown to be less than corresponding values for mild steel and greater than the corresponding values for aluminum sheet alloys. Failure modes for the (0<sub>2</sub>/+ - 60)<sub>s</sub> composite tubes are shown in Fig. 4. The Gr/Ep and G2/Ep tubes exhibited brittle modes of failure that consisted of extensive fiber splitting and ply delamination. The K/Ep tubes, on the other hand, failed in an accordion buckling mode similar to that obtained for metal tubes. Since a common matrix material was employed for all the drop tests, the differences in failure modes are directly related to the fiber failure characteristics. The graphite and glass fibers exhibited brittle fracture and splitting, while the Kevlar fibers had a more in elastic response with little fiber splitting.

The present work has shown that K/Ep continuous fiber composite materials are most

applicable for automotive structural members subjected to impact loads. The failure modes for the K/Ep material were more stable and repeatable than those for the Gr/Ep and G2/Ep composite. It should be realized, however, that only one deformation mode, axial crush, has been characterized by the above tests. Studies directed at combined bending and crush response of front structural automotive body components are discussed below.

#### BENDING PERFORMANCE OF COMPOSITE STRUCTURAL BEAMS

As illustrated in Fig. 5, energy absorption levels for front structural metallic body components are governed by the formation of plastic hinges for both upper and lower beam members. Since the axial impact experiments showed composite materials to fail via fiber fracture and delamination, static crush experiments for front structural composite body beams were conducted and compared with crush tests for baseline steel components. The front lower beam (Fig. 5) was selected for the experiments because it absorbed approximately four times the energy of the front upper beam in the illustrated static crush tests.

An individual steel front lower rail was initially crushed to provide baseline data. A cross head speed of 2.54 mm/sec was used for the steel beam crush test. Upon loading, the steel rail obtained a peak load of 55 kN before buckling and forming plastic hinges. The load level gradually decreased until the test was stopped at a crush displacement of 184 mm. The corresponding force-deflection curve (Fig. 6a) was integrated to determine that the steel rail absorbed 5.57 kN-m of energy.

Initial composite designs for the front lower rail component were based on service (elastic) loading conditions. Kevlar/Epoxy material was chosen because of the repeatable failure characteristics that were obtained from the tube impact tests. A fiber orientation of  $(+22)_{25}$  with respect to the beam axis matched the stiffness of the mild steel rail. The force-deflection response from statically crushing this eight-ply rail is compared to the steel curve in Fig. 6a. Both the peak load and post buckling force levels are below those of the steel design. Consequently, the energy absorption of the composite design was only 0.963 kN-m.

The poor behavior of the composite rail is due to its bending mode of failure. After crushing, there was little damage to the composite rail. As shown in Fig. 7, the only damage is a crease at the beam mid-span where bending took place. In order to reduce bending and enhance material crush toward the front section, the rail thickness was tapered by adding more plies where bending is likely. A  $(+22)_{25}$  Kevlar tapered rail was designed with seven segments, each containing a different number of plies. Eight plies were used near the bumper, followed by ten, twelve, sixteen, twenty, twenty-four, and thirty-two ply segments.

When this tapered front lower rail was statically crushed, the damage zone initiated at the rail front near the bumper. There was some delamination along with the bending which

occurred at the front of the rail. The post-buckling load level for the  $(+22)_{25}$  tapered rail was below that of the steel rail (Fig. 6a). Therefore, the energy absorption of the  $(+22)_{25}$  tapered composite rail was 2.98 kN-m, below the energy absorption level of the steel rail. By comparing the failure mode and postbuckling load level of the tapered composite rail, one could surmise that the increase in delamination in the tapered rail has caused an increase in the mean postbuckling load. In order to enhance this delamination, a  $(+45)_{25}$  tapered Kevlar design was fabricated with the same dimensions and number of plies as the  $(+22)_{25}$  tapered rail. The reason this design helps increase delamination is the existence of stress singularities between adjacent plies at the rail front edge. The singularities enhance the initiation and subsequent growth of delaminated regions.

During the crush of the  $(+45)_{25}$  tapered rail, the peak load was 50 percent higher than the peak loads of the steel and  $(+22)_{25}$  tapered rail (Fig. 6a). As crush of the segments with more than eight plies progressed, the force level increased significantly. With the larger mean load level, one would expect to have more rail delamination. Figure 8 shows that this is the case. The  $(+45)_{25}$  tapered Kevlar rail absorbed 9.02 kN-m of energy.

The untapered Kevlar rail was initially designed only for structural stiffness (service loads) and not for enhanced energy absorption. As such, it had a mass savings of 64 percent over the mild steel design. However, it absorbed 81 percent less energy than the steel design. Tapering the  $(+22)_{25}$  design increased the energy absorption of the rail by a factor of four, but the total energy absorption was still 21 percent less than the steel rail (Fig. 6b). The mass of the  $(+22)_{25}$  tapered rail increased by 50 percent over the untapered design. Finally, where changing the lay-up angle to  $+45$ , the energy absorption level of the composite rail exceeded that of the steel rail by 27 percent. However, the mass savings of the tapered design fell to 11 percent (Fig. 6b).

#### ONE-DIMENSIONAL DELAMINATION MODEL

**MODEL GEOMETRY** - The static crush tests of the Kevlar rails have shown that delamination is the primary failure mechanism on the compressively-loaded beam face. A one-dimensional beam-plate model was applied to study delamination buckling and growth. The model configuration consists of a homogeneous, orthotropic beam-plate of thickness  $T$  and of unit width containing a single delamination at depth  $H$  ( $H \leq T/2$ ). As shown in Fig. 9, the plate is clamped-clamped and subjected to an axial compressive force  $P$  at the ends  $x = \pm L$ . The delamination extends over the interval  $-l \leq x \leq l$ . Over this region the laminate consists of two parts, the part above the delamination, of thickness  $H$ , referred to the "upper" part and the part below the delamination of thickness  $T-H$ , referred to as the "lower" part. The remaining laminate outside the interval  $-l \leq x \leq l$  and of thickness  $T$ , is referred to as the "base" laminate. The

separate parts are shown in Fig. 10.

When the laminate is loaded, three different modes of instability can be identified, as shown in Fig. 11. First, global buckling of the whole beam may occur before any other deflection pattern takes place. Secondly, both local and global buckling involving the upper and lower parts as well as the base plate may occur. This mode is referred to a "mixed buckling". Thirdly, only local buckling of the delaminated upper layer may occur while the lower part and base plate remain flat.

**DELAMINATION STABILITY** - The problem of delamination buckling was formulated and solved by applying the perturbation or small parameter method. The method consists of developing the solution in powers of a parameter which either appears explicitly in the problem or is introduced artificially. Details of the formulation and solution procedure are presented in [4].

Numerical results for delamination buckling are presented for K/Ep, Gr/Ep, and G/Ep composites. The elastic constants typical of these materials are listed in Table 4. It is assumed that the filaments are parallel to the x-axis. The different regions of buckling instability can be identified in the plots of the critical instability load, normalized with respect to the Euler load for the delaminated layer,  $4\pi^2 E_1 H^3 / 12(1 - \nu_{13}\nu_{31}) L_d^2$ , vs. delamination length for different composite materials (Fig. 12). For short delamination lengths, global buckling is dominant, while for relatively large lengths local buckling of the delaminated layer occurs first. As shown in Fig. 12, the range of the different instability modes is not affected by the composite type, while an increased instability load for the higher modulus Gr/Ep, material is expected. The effect of lay-up angle on a symmetric (\*a) laminate is shown in Fig. 13. As expected, the buckling load decreased with increasing lay-up angle because of reduced laminate stiffness in the x-direction.

**DELAMINATION GROWTH** - The process of delamination growth which takes place after delamination buckling can be analyzed on the basis of a Griffith-type fracture criterion. Predicting whether the delamination will grow requires evaluation of the energy-release rate. This quantity is the differential of the total potential energy with respect to delamination length [5]. Alternatively, a J-integral concept may be used to compute the energy-release rate from stress and displacement distributions near the delamination. The latter method was applied to a one-dimensional delamination [6] and resulted in an algebraic expression for the energy release rate in terms of the axial forces and bending moments acting across the various cross sections adjacent to the delamination tip. This expression was modified in [4] to account for effects of transverse shear forces.

In terms of the quantities

$$P^* = P (H/T) - P_u$$

$$M^* = M_u$$

$$M^{**} = P^*T/2 - M^* \quad (4)$$

where  $P_u$  and  $M_u$  are as shown in Fig. 10, the energy release rate can be expressed as

$$G = \frac{12(1 - \nu_{13}\nu_{31})}{2E_1 H} \left[ P^{*2} + 12(M^*/H)^2 \right. \\ \left. \left[ 1 - \alpha P^*/(A_u G) \right]^2 \right] + \frac{12(1 - \nu_{13}\nu_{31})}{2E_1 (T - H)} \\ \left[ P^{*2} + 12[M^{**}/(T - H)]^2 \right] \left[ 1 + \alpha P^*/(A_1 G) \right]^2 \quad (5)$$

The relation between the nondimensional energy-release rate,  $G = G/(ET^5/L^4)$  and the applied load normalized to be independent of delamination length,  $P = P/[4\pi^2 E_1 T^3 / 12(1 - \nu^2)L^2]$  is plotted in Fig. 14 for three lay-up angles. Scales of the same length for the applied load (corresponding to a different critical load for each case) have been used. The important feature is the increase in slope of the G-P curves with the greater lay-up angles. This means that growth could occur earlier and that these will potentially absorb more energy since the energy released per unit applied load is higher. This trend correlates with the results of the static bend tests which showed greater lay-up angles to be more energy absorbent than rails with lower lay-up angles.

#### SUMMARY AND CONCLUSION

The present study has focused on the effects which material type and angle-ply lay-up have on the failure of composite tubes subjected to compressive impact loads and composite rectangular beams undergoing bending loads. Three composite materials systems were used for the impact tests: graphite/epoxy (Gr/Ep), Kevlar/Epoxy (K/Ep), and glass/epoxy (GL/Ep). Results for energy absorption varied significantly as a function of lay-up angle and material type. The Gr/Ep and K/Ep angle-ply tubes exhibited specific energy absorption values that were greater than or equal to corresponding values for steel and aluminum materials. Gr/Ep and GL/Ep had brittle fracture modes of failure, whereas the K/Ep angle-ply tubes collapsed in a repeatable accordion buckling mode. Experimental studies to characterize the bending performance of composite beams showed that delamination is the primary failure mechanism for the compressively loaded beam face. A (\*22°) untapered beam, designed to carry service (elastic) loads, had a mass savings of 64 percent over a steel design, but absorbed 81 percent less

energy than the steel design. Tapering the beam thickness and changing the lay-up from 22° to 45° to enhance delamination increased the beam energy absorption to a level which exceeded that of the steel design by 27 percent. However, mass savings of the composite design fell to 11 percent. Finally, a one-dimensional beam-plate model was formulated to investigate phenomenological aspects of delamination buckling and growth. Energy release rate values for delamination growth exhibited trends which correlated with energy absorption levels obtained from the static crush tests.

#### ACKNOWLEDGMENT

The authors wish to thank L. Wickliffe and P. Watling for conducting the tube impact and beam bending experiments.

#### REFERENCES

1. Farley, Gary L., "Energy Absorption of Composite Materials," *J. Composite Materials*, **17**, 267-279 (1983).
2. Thornton, P. M., "Energy Absorption in Composite Structure," *J. Composite Materials*, **13**, 247-262 (1979).
3. N. Draper and H. Smith, "Applied Regression Analysis," Wiley, New York, New York (1981).
4. Kardomateas, George and David W. Schmueser, "Effect of Transverse Shearing Forces on Buckling and Postbuckling of Delaminated Composites Under Compressive Loads," General Motors Research Publication GMR-5679 (1987).
5. Chai, H., C. D. Babcock and W. G. Knauss, "One Dimensional Modeling of Failure in Laminated Plates by Delamination Buckling," *Int. J. Solids Structures*, **17**, 1069-1083 (1981).
6. Budiansky, B. and J. R. Rice, "Conservation Laws and Energy Release Rates," *J. Appl.*, **40**, 201-203 (1973).

Table 1 -- Composite Prepreg Materials

<u>Fiber/Matrix</u>	<u>Nominal Cured Ply Thickness, mm</u>	<u>Material Type</u>
T300/5208	0.175	Tape
Kevlar 49/5208	0.197	Tape
S-Glass/5208	0.158	Tape

Table 2 -- Composite Tube Data

Laminate Construction	Graphite Epoxy		Kevlar/Epoxy		Glass/Epoxy	
	Number of Plys	Wall Thickness mm	Number of Plys	Wall Thickness mm	Number of Plys	Wall Thickness mm
(0°) <sub>8</sub>	8	1.27	8	1.57	8	1.32
(90°) <sub>8</sub>	8	1.27	8	1.57	8	1.32
(0 <sub>2</sub> °/+30°) <sub>8</sub>	8	1.40	8	1.65	8	1.38
(0 <sub>2</sub> °/+45°) <sub>8</sub>	8	1.40	8	1.65	8	1.38
(0 <sub>2</sub> °/+60°) <sub>8</sub>	8	1.40	8	1.65	8	1.38
(0 <sub>2</sub> °/+90°) <sub>8</sub>	8	1.40	8	1.65	8	1.38

Table 3 -- Summary of Weighted Least Squares Regression Analysis

Material	Angle (Deg)	Predicted Least Squares Value (N-m/Kg)	95 Percent C.I. for Predicted Value (N-m/Kg)
Glass	30	6,864	+ 345
Glass	45	9,129	+ 205
Glass	60	11,393	+ 408
Glass	90	15,921	+1009
Kevlar	30	13,285	+1433
Kevlar	45	14,109	+1001
Kevlar	60	14,932	+1269
Kevlar	90	16,579	+2792
Graphite	30	25,126	+1680
Graphite	45	25,949	+1316
Graphite	60	26,773	+1515
Graphite	90	28,410	+2898

Table 4 -- Material Constants

Material	$E_{\ell t}$ GN/m <sup>2</sup>	$R_t$ GN/m <sup>2</sup>	$G_{\ell t}$ GN/m <sup>2</sup>	$\nu_{\ell t}$
Graphite-Epoxy	215	6.5	3.2	0.26
Kevlar-Epoxy	70	4.5	2.5	0.35
Glass-Epoxy	53	14	8.6	0.26



FIG. 1 DROP TOWER TEST FACILITY

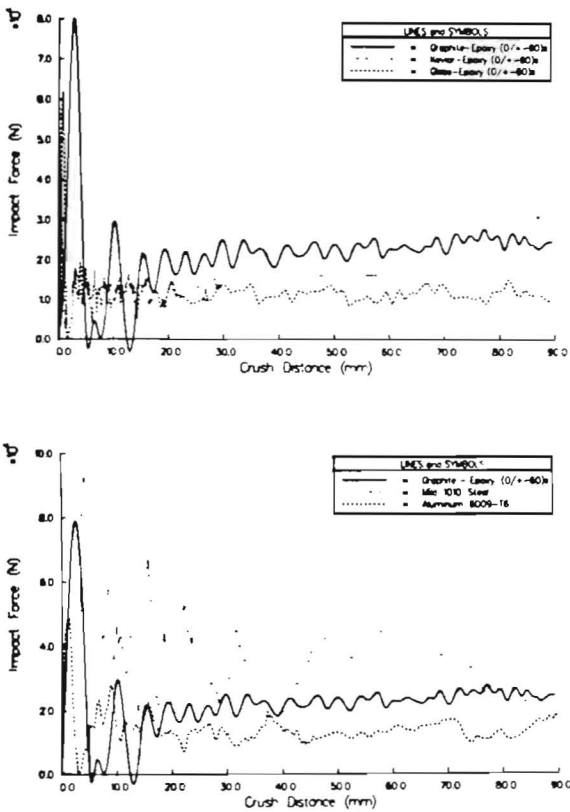


FIG. 2 FORCE-DEFLECTION RESPONSE FOR IMPACTED COMPOSITE AND METAL TUBES

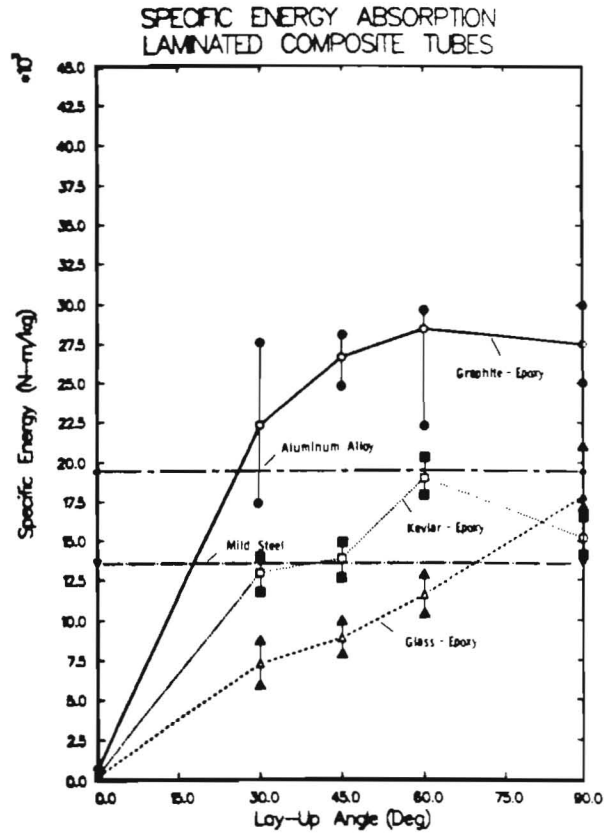


FIG. 3 EFFECT OF LAMINATE CONSTRUCTION ON DYNAMIC SPECIFIC ENERGY ABSORPTION

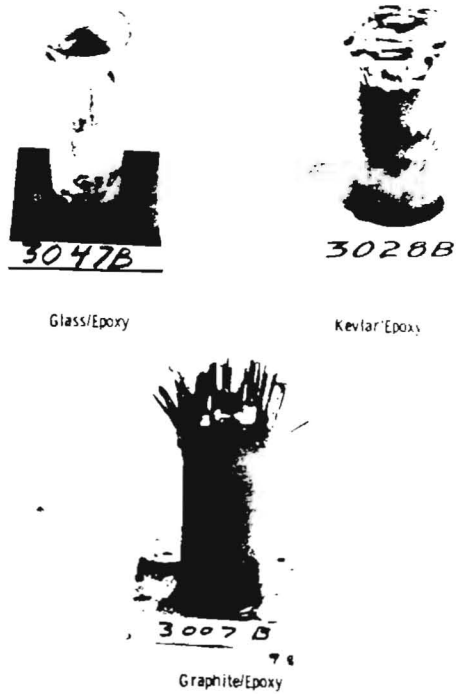


FIG. 4 FAILURE MODES FOR IMPACTED  $(0_2/\pm 60)_S$  TUBES



FIG. 5 PLASTIC HINGE FORMATION FOR STATIC CRUSH OF MILD STEEL STRUCTURE

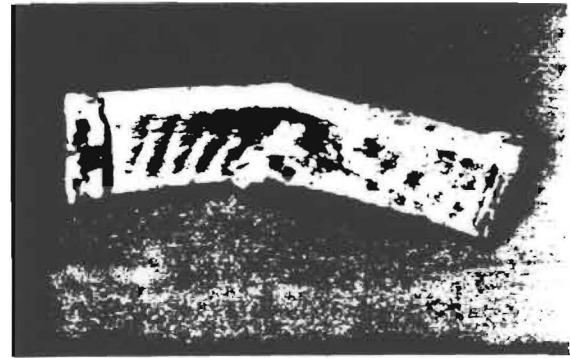


FIG. 7 FAILURE AT MIDSPAN OF ( $\pm 22^\circ$ ) KEVLAR/EPOXY BEAM

FORCE DEFLECTION RESPONSE FOR STATIC CRUSH OF STEEL SPACE FRAME AND CRUSHER TESTS OF FRONT LOWER RAILS

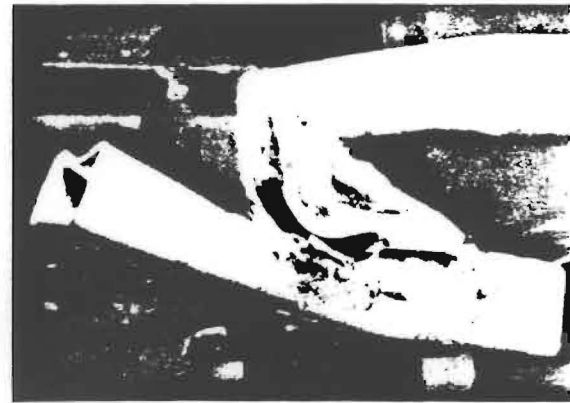
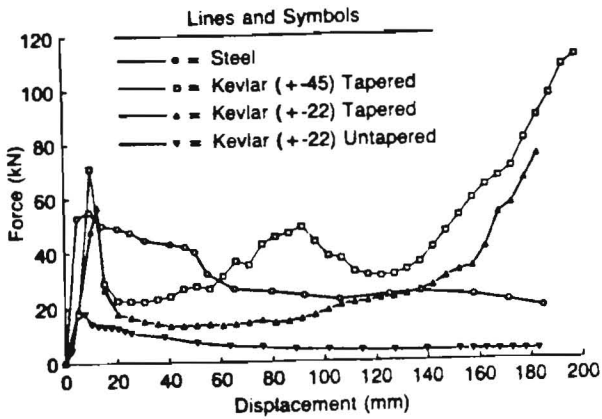


FIG. 8 PROGRESSIVE DELAMINATION FAILURE OF ( $\pm 45^\circ$ ) KEVLAR/EPOXY TAPERED BEAM

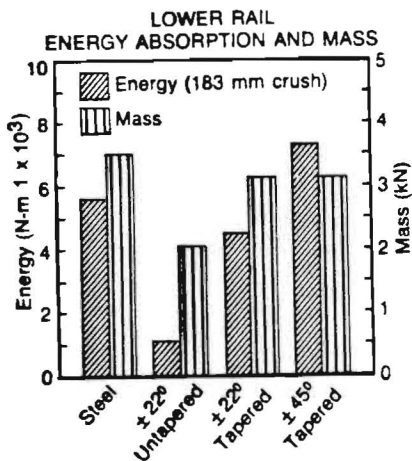


FIG. 6 FORCE-DEFLECTION RESPONSE AND ENERGY ABSORPTION LEVELS FOR COMPOSITE FRONT LOWER RAILS

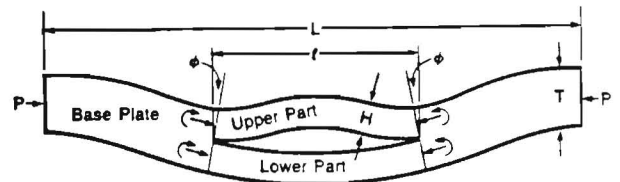


FIG. 9 DELAMINATION/BUCKLING GEOMETRY

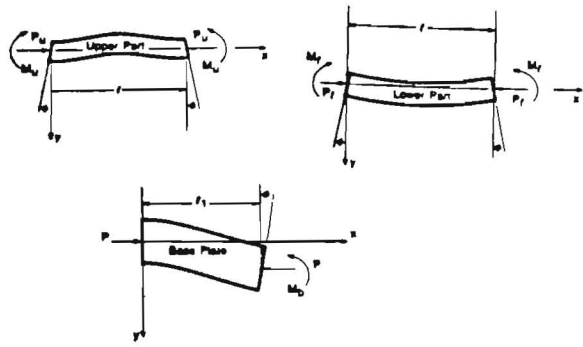


FIG. 10 DEFINITION OF DELAMINATION SEGMENTS

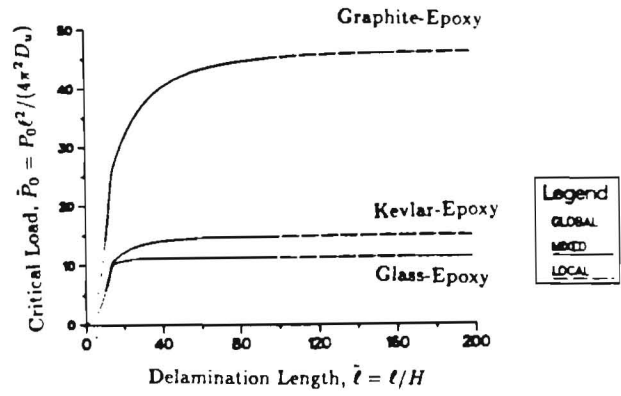


FIG. 12 CRITICAL (BUCKLING) FORCE VS. DELAMINATION LENGTH FOR DIFFERENT MATERIALS ( $T/H=15$ ,  $L/H=200$ )

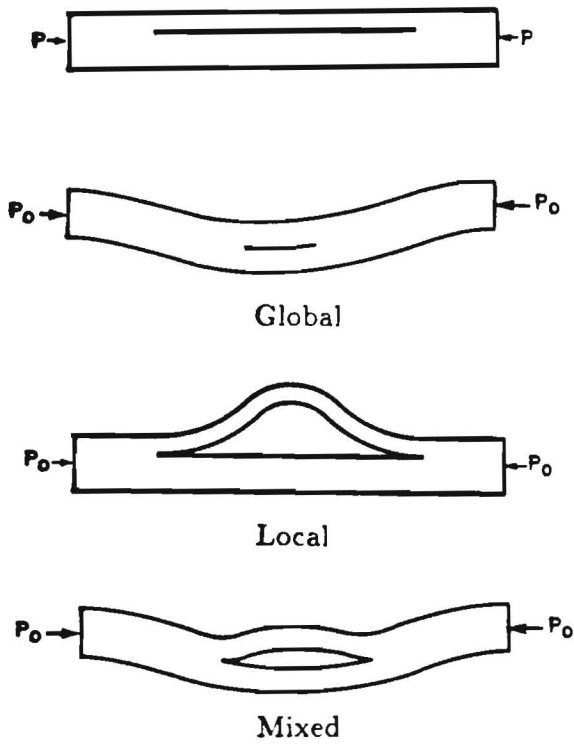


FIG. 11 INSTABILITY MODES FOR A DELAMINATED COMPOSITE

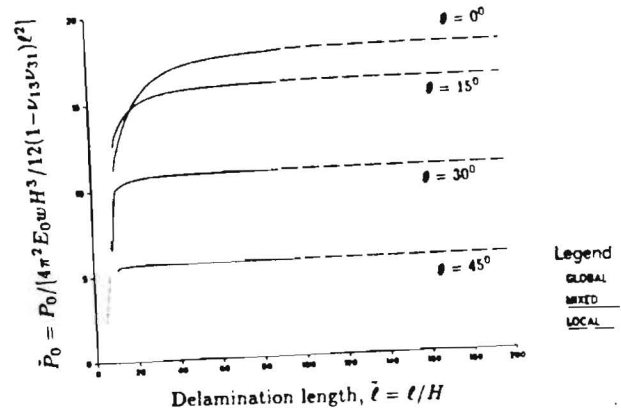


FIG. 13 EFFECT OF LAY-UP ANGLE ON BUCKLING LOAD ( $T/H=18$ ,  $L/H=200$ )

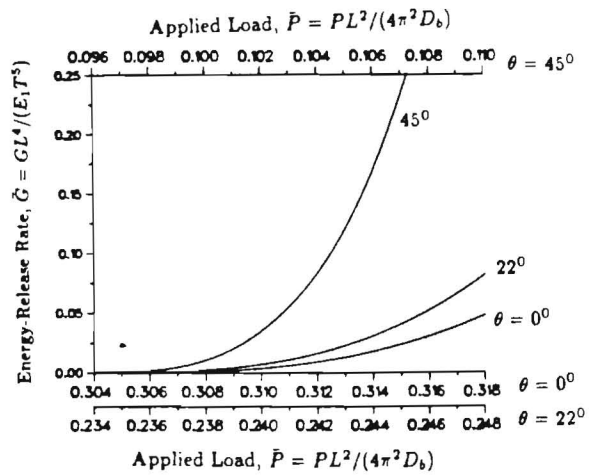


FIG. 14 EFFECT OF LAY-UP ANGLE ON STRAIN ENERGY RELEASE RATE (KEVLAR  $\pm \beta_S$ ,  $T/H=6$ ,  $L/H=200$ )